MODELLING ATMOSPHERIC RADIATIVE TRANSFER CONDITIONS AND ITS COMPARISON TO EMPIRICAL SOLAR IRRADIANCE IN SOUTH AFRICA

Charles H. Fourie[1], Hartmut Winkler[2], and Kittessa Roro[3]

[1] Department of Physics, University of Johannesburg, PO Box 524, 2006 Auckland Park, Johannesburg, South Africa;

E-Mail: 201049523@student.uj.ac.za

[2] Department of Physics, University of Johannesburg, PO Box 524, 2006 Auckland Park, Johannesburg, South Africa; Phone: +27-11-5594417; Fax: +27-11-5592339; E-Mail: hwinkler@uj.ac.za

[3] Council of Scientific and Industrial Research, Pretoria South Africa, CSIR-Department of Energy, E-mail: kroro@csir.co.za

Abstract

This paper seeks to investigate the performance of solar irradiance modelling to ground based data in an urban environment. The ability to accurately model and in turn determine solar irradiance as it propagates through the atmosphere, and predict the potential for renewable energy application, has lured investment opportunities and has become a topic of interest over the past couple of years as the price of solar panels have dropped. Modelling here is done with SMARTS 2.9.5, a cost free open source modelling program. This investigation analyses and compares the performance of the SMARTS model, using a varying complexity of input parameters, to see under which conditions the model best simulates results gathered by ground instrumentation based in Pretoria, South Africa.

Keywords: Solar Irradiance, SMARTS, Aerosol optical depth, South Africa, Highveld.

1 Introduction

Solar potential pertaining to electrical power generation relies not only on the quantity but also the spectral distribution of solar irradiance or sunlight at ground level. As solar irradiance (usually in the form of a beam of direct sunlight) propagates through the atmosphere it undergoes various interactions with airborne particulates, which causes the light beam to scatter and diffuse. The intensity or effect of these interactions determine both quantity and spectral distribution of light reaching the ground and will be discussed in more detail in the chapters that follow. The ability to accurately predict and model the ground-level spectral distribution of sunlight has been a topic of great interest and continues to escalate following the ever-increasing effort to minimise global warming accompanied by local and global investment opportunities in renewable energy.

Typically, there are two dominant methods of determining the viability of a region to invest in solar energy. The most broadly used method is based on satellite monitoring data combined with historical data to estimate the probability of a region receiving a certain amount of solar irradiance. The second method, which this paper will be investigating, is using a computational model with direct comparison to solar irradiance as measured by ground-based instrumentation.

2 Solar Irradiance

2.1 Spectrum

Extra-Terrestrial irradiance emitted by our sun is well understood, with an effective surface temperature of around 5800 K, it has been described as a quasi-static blackbody with a broad spectrum with most of the emitted radiation covering the Ultra-violet (UV: 0.28-0.4 μm), Visible region (VIS: 0.4-0.7 μm) and Near- infrared / Infrared (NIR/ IR: 0.7–3.0 μm) [1].

2.2 Solar Constant

Total solar irradiation (*TSI*) at the top of the Earth's atmosphere undergoes little variation, despite sudden and periodic temporal changes caused by sunspots (cooler parts typically indicated by a dark spot) or similar facets of the solar cycle, which has a period of 11 years. Solar intensity at the top of the atmosphere (TOA) has been calculated by the National Renewable Energy Laboratory, equating to a solar constant (SC) of approximately 1361.2 W/m^2 with seasonal variations brought on by solar geometry[2].

2.3 Solar Geometry

Extra-Terrestrial radiation (*ETR*) is the total solar irradiance available at the top of the atmosphere and is calculated using the Total Solar Irradiation (*TSI*)

$$ETR = TSI * \left({}^{r_0}/_{r}\right)^2 \qquad (1)$$

where r_0 is the annual mean distance between the Earth and the Sun and r is the Earth-Sun distance.

2.4 Solar geometry and the atmosphere

The Earth's angle of inclination relative to the orbital plane, combined with the inherent properties of a rotating sphere, means that at any given moment a photon of light would not always pass through a uniform volume of atmosphere. Instead the optical path depends on the (time-dependent) Earth's position and orientation relative to the Sun. These factors are represented by Solar Azimuth angle (*SAA*), Solar-Zenith angle (*SZA*) and relative Airmass (*AM*). The solar azimuth angle corresponds to the angle between true north and the solar position along the plane of the orbit. Airmass is approximated by taking the cosine of the solar zenith angle, which gives the amount of atmosphere (in terms of vertical atmospheric thickness) the direct solar beam must pass through to reach the ground.

3 Solar Irradiance Monitoring

3.1 Ground monitoring

Due to the high variability of aerosols, ground monitoring remains a crucial part when it comes to modelling solar irradiance of the interior of South Africa. One of the major contributors to better understanding the atmospheric constituents and its impact on solar irradiance in Southern Africa was driven by the South African Universities Radiometric Network (SAURAN). This project aimed to establish a high-resolution network of multiple ground-based monitoring stations. The stations were designed to measure Direct Normal Irradiance (DNI), Global Horizontal Irradiance (GHI) and Diffuse Horizontal Irradiance (DHI) at one-minute intervals. [3]

The information provided by SAURAN has been highly beneficial to projects such as determining the viability of solar resources in Durban [4] and the potential for concentrated solar power in South Africa [5]

4 Instrumentation

4.1 CSIR

The instrumentation required was supplied by the CSIR, which also allowed the use of the data. Irradiance data was gathered using the following:

- Pyranometer (Kipp & Zonen), provided information regarding Global Horizontal Irradiance (GHI) as well as Diffuse Horizontal Irradiance (DHI), measured from 280 nm to 2800 nm at a frequency of 30 seconds and recording data every minute.
- Pyrheliometer (Kipp & Zonen), provided information regarding Direct Normal Irradiance (DNI), measured from 200 nm to 4000 nm at a frequency of 5 seconds and recording data every minute.
- Spectroradiometer (EKO-Weiser), provided information regarding Direct Normal Irradiance (DNI), measured from 283 nm to 1100 nm at a frequency of 5 seconds and recording data every minute.
- Weather data was gathered by an integrated weather sensor (Thies Clima) and recorded wind data, temperatures, humidity and precipitation at 30 second intervals.

4.2 AERONET

Atmospheric data was also obtained from the Aerosol Robotic Network (AERONET) database. The AERONET project is a multi-national collaboration and consists of a ground-based remote aerosol sensing network. The collaboration provides globally distributed observations such as spectral Aerosol Optical Depth (AOD). Raw data is captured at each station and transmitted for quality processing. The data can be viewed on three levels, level 1.0 "unscreened", 1.5 "cloud-screening and quality controlled" and thirdly level 2.0 "quality assured". [7]

AERONET uses CIMEL Electronique CE318 multiband sun photometers that perform measurements of sky radiance and spectral solar irradiance. The AERONET station whose data is used here is located within the grounds of the CSIR, approximately 700 m south of the Spectroradiometer, with less than 30 m of vertical difference between the two locations.

5 Data collection

5.1 CSIR

Weather data utilised for the analysis were: temperature, relative humidity, daily average temperature and temperature, all for the time of simulation.

The CSIR has a permanent monitoring station which measures various meteorological and irradiance parametric data. The frequency of the measurements is set to one-minute intervals. The data relevant to the study has been included in Table 1.

Function	Abbreviation	Unit
Irradiance	GHI	W/m^2
	DNI	
	DIF	
Temperature	Temperature	°C
Wind	Velocity	m/s
	Direction	°
Air Pressure	BP_Avg	mbar

Table 1: Information provided by the CSIR Energy department.

The Spectroradiometer performs a "sweep" from 280 nm through to 1100 nm measuring irradiance. The instrumentation was set to capture data in "RAW" mode, which resulted in an inconsistent step size ranging roughly from 0.37 nm to 0.49 nm, which was then adapted to 1 nm interval step-size by means of rounding with correlated sample averaging. The measurements were conducted at one-minute intervals.

5.2 AERONET

AOD data was obtained using the download tool on the AERONET website, which allows the user to specify the desired timeframe, data quality level and data type. For this investigation level 2.0 data was used and all data points were specified for aerosol optical depth with precipitable water vapour and Ångstrom parameter. The website also provides additional useful irradiance-linked parameters such as the "AERONET Inversion Data Product", which include: size distribution, Single Scattering Albedo and Asymmetry. [8]

6 Modelling & Preparation

6.1 SMARTS preparation

The "Simple Model for the Radiative Transfer of Sunshine" (SMARTS) was developed by Christian. A. Gueymard [6] and is written in FORTRAN. SMARTS was used because of its ability to predict direct beam, diffuse and global horizontal irradiance at the Earth's surface, as well as simulate irradiance as measured by instrumentation such as a Spectroradiometer, Pyrheliometer and a Pyranometer found at the CSIR.

The version used in this investigation (SMARTS code, version 2.9.5) is an updated version of the original SMARTS model. SMARTS has revised the algorithm to calculate direct beam radiation. More accurate transmittance and extinction parameters are introduced, along with effects caused by temperature and humidity. SMARTS calculates and estimates the solar spectral irradiance as it propagates through the atmosphere according to extinction parameters under cloudless atmospheric conditions, such as Rayleigh scattering, aerosol absorption, and extinction by ozone and mixing gases associated with water vapour and nitrogen dioxide [4]. SMARTS provides the user with the ability to input ground meteorological data. Alternatively, the user may choose one of ten prescribed reference atmospheres followed by nine reference aerosol models. The user is also provided with the option of entering Ångstrom exponents above and below 500nm (α_1, α_2), coupled with corresponding single-scattering albedo (Ω) and the asymmetry factor g.

The SMARTS program utilises a series of "Cards" designed to generate an input file before the program is run. Each card provides the user with input and data handling options. In total there are 17 main cards with subdivisions within each card. Due to the variability within the card parameters certain cards were kept constant, while cards not mentioned in Table 2 or Table 3 were bypassed as they would typically restrict the inputs. Variables which remained constant for each day can be seen in Table 2 below.

Card	Purpose	Value
6	Gaseous absorption	Pristine atmosphere
7	Carbon dioxide	370 ppmv
10	Albedo	Concrete slab
11	Spectral range	280-2800nm
12	Output	DNI

Table 2: Input cards with their corresponding fixed values.

Cards which were specific to each of the days selected can be seen in the Table 3 below.

Card	Purpose
1	Comments
2	Site pressure
3	Atmosphere
4	Water vapour
5	Ozone
8	Aerosol model
9	Turbidity
17	Solar geometry

Table 3: Input cards with varied input dependent on the selected day.

6.2 AERONET

Once the data had been collected it was sorted according to months. For each chosen day the entire week spanning from three days prior to three days past would be selected, i.e. data for the 25th of April would consist data of days from the 22nd of April until the 28th of April for each year from 2012 through to 2015. The selected information would be sorted according to corresponding solar zenith angle and relevant time of the day. The data would then be processed to indicate average values, variance and mean values.

D: M: Y	Time (Local)	SZA (deg)
25 04 2018	12:05:00	38.98
05 05 2018	12:03:00	42.04
08 05 2018	12:03:00	42.87
26 05 2018	12:04:00	46.89
02 06 2018	12:05:00	47.95
06 06 2018	12:05:00	48.41
16 06 2018	12:08:00	49.09
27 06 2018	12:10:00	49.06
02 07 2018	12:11:00	48.77
18 07 2018	12:13:00	46.74
23 07 2018	12:13:00	45.78
28 07 2018	12:14:00	44.69
01 08 2018	12:13:00	43.72

Table 4: Selected dates, times and solar zenith angle chosen to test SMARTS.

Tests for each of the selected days were conducted using data from the CSIR and categorised as static or non-variable input data. Data from AERONET was not recorded on the same day as that collected by the CISR instrumentation, but instead relied on historical values which had been recorded during the same time of year from 2012 through to 2015, which resulted in the data being treated as variable.

6.3 CSIR Data Preparation

The data collected by the spectroradiometer was compared at 1 nm intervals ranging from 280 nm to 1100 nm and compared to the SMARTS simulated results using the Root Mean Square Error (RMSE). The data collected by the pyranometer and the pyrheliometer was assessed using broadband values ranging from 280 nm to 2800 nm and 280 nm to 4000 nm and compared to simulated broadband values generated by SMARTS.

6.4 Modelling

First each day was modelled using averaged values for AOD, Ångstrom exponents and Ozone Dobson values obtained for the period described in 6.2, the values can be seen in Table 5. The modelled data was then compared to the measured data. Then individual data obtained from AERONET would be used as input parameters to minimise the margin of error. If the model underpredicted, conditions for days with lower aerosol optical depth values would be tested and evaluated. Likewise, if the model overpredicted days with higher aerosol optical depths would be similarly treated. Once a fair fit had been established, the Ångstrom exponent would be adjusted. Lowering the α_1, α_2 value would result in an increase below 500 nm and a decrease above 500nm with little effect on the total irradiance.

7 Results

7.1 Determination of Clear Sky days

Clear-sky days were determined using GHI intensity throughout the day to eliminate days with full or scattered cloud cover. If upon visual inspection the day exhibited drops in intensity characteristic of cloud cover, the day would be discarded. An example of a "typical" clear day can be seen in Figure 1.

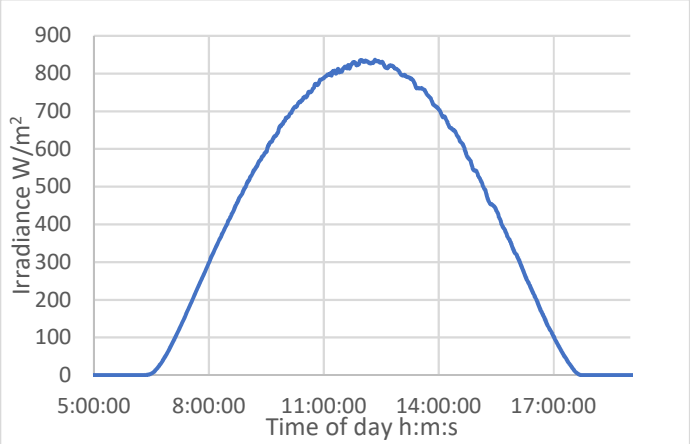

Fig 1: Global horizontal irradiance GHI curve for a clear-sky day for 25 April 2018

7.2 AERONET

At the time of this investigation the CIMEL Electronique CE318 multiband sun photometer had just been sent back to NASA for scheduled maintenance and re-calibration. Live or time accurate data could not be obtained for the period spanned by the investigations. An attempt was made to utilise the level 2.0 data from 2012 through to 2015. This would provide values "typical" for the selected period of the year.

D: M: Y	τ 500nm	α (380-500nm)	α (500-870nm)
25 04 2018	0.098	1.64	1.26
05 05 2018	0.131	1.69	1.31
08 05 2018	0.164	1.63	1.44
26 05 2018	0.174	1.59	1.46
02 06 2018	0.134	1.56	1.36
06 06 2018	0.106	1.37	1.21
16 06 2018	0.121	1.33	1.29
27 06 2018	0.109	1.49	1.27
02 07 2018	0.190	1.53	1.48
18 07 2018	0.140	1.47	1.54
23 07 2018	0.148	1.38	1.32
28 07 2018	0.132	1.30	1.26
01 08 2018	0.155	1.35	1.27

Table 5: AERONET data from 2012-2015.

7.3 Findings

The time at which the measurements at the CSIR were conducted varied seasonally. On the the 25th of April solar noon was at 12:05:00, with the earliest instance of solar noon at 12:03:00 on the 5th and 8th of May and a latest occurrence at 12:13:00 on the 1st of August. Weather data for the time of measurement during the period from April through to August did not vary greatly, ranging from a maximum temperature in April of 24.9 °C at the time of measurement to a minimum in July of 14.1 °C at the time of measurement. Average daily temperatures varied with season but ranged correspondingly with the highest daily average temperature in April of 23.9 °C and a minimum in July of 10.35 °C, more detailed values can be seen in the Table 6. The information presented in Table 6 were initially the only input parameters in the initial testing and were kept constant as more detailed parameter were introduced.

D: M: Y	Time	Temp °C	RH %	Pressure mbar
25 04 2018	12:05	24.90	41.01	866
05 05 2018	12:03	22.60	20.91	866
08 05 2018	12:03	22.05	34.96	865
26 05 2018	12:04	22.65	33.49	866
02 06 2018	12:05	19.67	24.96	867
06 06 2018	12:05	17.62	36.45	871
16 06 2018	12:08	18.46	33.27	865
27 06 2018	12:10	16.59	42.36	868
02 07 2018	12:11	19.67	26.98	863
18 07 2018	12:13	14.10	41.51	874
23 07 2018	12:13	17.00	44.41	875
28 07 2018	12:14	22.48	23.66	867
01 08 2018	12:13	22.35	28.06	862

Table 6: Values for temperature, relative humidity and air pressure at time of measurement for each of the select days.

Broadband irradiance values measured for each day at the time specified in Table 6 can be seen in Table 7 and Table 8 below, followed by those which had been calculated by SMARTS.

D: M: Y	GHI	DHI	DNI
25 04 2018	835.1	79.1	954.2
05 05 2018	794.1	61.1	972.2
08 05 2018	774.6	82.0	929.5
26 05 2018	706.2	72.8	911.2
02 06 2018	726.7	53.3	992.8
06 06 2018	640.3	113.6	778.0
16 06 2018	691.4	56.4	951.7
27 06 2018	641.6	120.7	780.5
02 07 2018	675.8	91.7	867.7
18 07 2018	711.2	87.8	895.2
23 07 2018	735.2	67.4	941.3
28 07 2018	722.4	89.2	872.6
01 08 2018	761.3	81.4	922.6

Table 7: Measured broadband irradiance values (in W/m^2) at the times given in Table 6.

D: M: Y	GHI	DHI	DNI
25 04 2018	829.7	77.1	968.3
05 05 2018	784.4	61.8	972.9
08 05 2018	774.0	88.3	935.5
26 05 2018	696.5	74.4	910.2
02 06 2018	715.0	54.9	985.3
06 06 2018	657.0	112.6	819.9
16 06 2018	673.9	54.4	945.9
27 06 2018	666.6	123.1	829.3
02 07 2018	672.5	93.6	878.0
18 07 2018	682.3	77.6	882.2
23 07 2018	717.1	72.4	968.3
28 07 2018	701.5	72.9	972.9
01 08 2018	741.1	72.0	935.5

Table 8: Broadband irradiance values modelled by SMARTS (in W/m^2).

Using aerosol and Ångstrom values from AERONET resulted in SMARTS underpredicting both broadband and spectral irradiance by a significant factor. The results in Table 8 were obtained using the Aerosol optical depth and Ångstrom parameter values in Table 9. SMARTS simulations were conducted for each of the selected days using fixed input values from Table 6 with varying values such as aerosol optical depth at 500 nm, average Ångstrom exponent α_1 below and α_2 above 500 nm.

D: M: Y	τ (500nm)	α_1	α_2
25 04 2018	0.025	0.90	0.70
05 05 2018	0.040	0.30	0.25
08 05 2018	0.055	0.60	0.50
26 05 2018	0.050	0.00	0.00
02 06 2018	0.005	0.00	0.00
06 06 2018	0.140	1.00	0.70
16 06 2018	0.020	0.00	0.00
27 06 2018	0.115	0.00	0.30
02 07 2018	0.100	1.20	0.90
18 07 2018	0.080	0.50	0.20
23 07 2018	0.045	0.50	0.40
28 07 2018	0.090	0.30	0.18
01 08 2018	0.055	0.30	0.25

Table 9: Aerosol optical depth and Ångstrom values used to simulate the conditions for each day.

Fig. 2, Fig. 3 and Fig. 4 depict some of the spectral representations made by SMARTS using input values from Table 6 and Table 9, compared that measured by the CSIR.

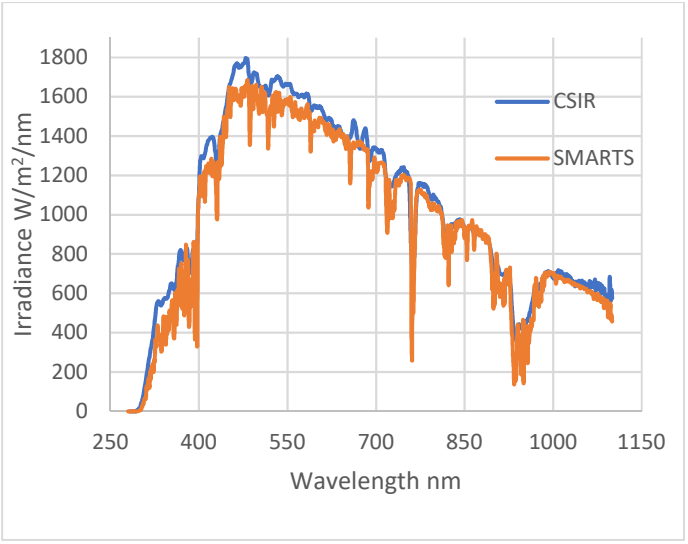

Fig 2. Direct Normal Irradiance DNI (W/m^2/nm) as measured by the Spectroradiometer and modelled by SMARTS, for 25 April 2018

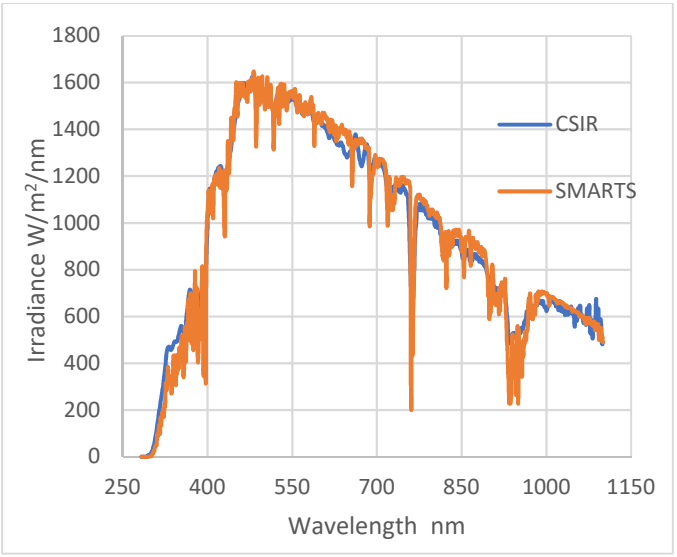

Fig 3. Direct Normal Irradiance DNI (W/m^2/nm) as measured by the Spectroradiometer and modelled by SMARTS, for 2 June 2018.

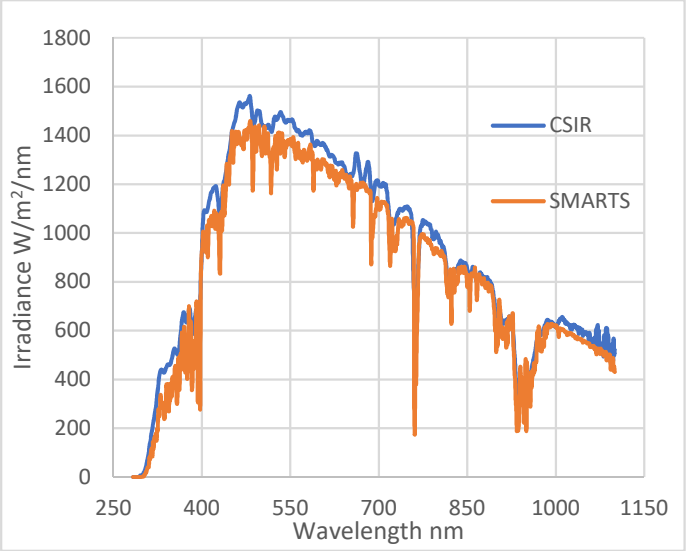

Fig 4. Direct Normal Irradiance DNI (W/m²/nm) as measured by the Spectroradiometer and modelled by SMARTS, for 2 July 2018.

7.4 Analysis

Each dataset from the spectroradiometer was compared to that as modelled by SMARTS using the root mean square error.

$$RMSE = \sqrt{\frac{\sum_{i=280}^{1100}(Modelled_i - Measured_i)^2}{820}} \qquad (2)$$

The RMSE values were affected by regions of poor fit, particularly by the UV: 280 – 400 nm region which has proven to be difficulty to measure with a certain degree of accuracy. Another area which affected the RMSE was the O_2 absorption band which can be seen at 760 nm and could not be adjusted or manipulated directly. However, once a satisfactory RMSE value had been achieved the measured and modelled broadband irradiance values were compared using relative percentage of modelled over measured as can be in Equation 3 - 5.

$$GHI\ \% = \frac{GHI_{modelled}}{GHI_{measured}} \qquad (3)$$

$$DNI\ \% = \frac{DNI_{modelled}}{DNI_{measured}} \qquad (4)$$

$$DHI\ \% = \frac{DHI_{modelled}}{DHI_{measured}} \qquad (5)$$

To test the quality of the results further, the angle SZA_1 was calculated from measured broadband irradiance and compared SZA_2, these values were accurate to within 0.02 %. These values were calculated from the broadband irradiance of the modelled spectra using Equation 6 and 7

$$SZA° = arccos\left(\frac{GHI - DHI}{DNI}\right) * \frac{\pi}{180°} \qquad (6)$$

$$SZA\ \% = \frac{SZA_{modelled}}{SZA_{measured}} \qquad (7)$$

8 Discussion

8.1.1 SMARTS Fitting

Despite the lack of time-overlapping data from AERONET to that measured by the CSIR, the use of daily averages drawn from the specified 3 day before and after range for 2012-2015 provided a reasonable fit. Utilising the built in atmospheric functions also provided a good fit for certain days and could serve to provide rudimentary predictions. The model is simple to use and provides the user with a great variety of ways to run each simulation.

The months of April and May were more difficult to fit, presumably due to the higher moisture levels in the atmosphere. However, utilising the water vapour absorption instead of having the model calculate it from temperature and relative humidity provided a better convergence. The lack of certainty in water vapour estimation is not considered a major drawback in this investigation as the spectral regions affected by water vapour are in the infrared, where solar spectral irradiance is not very strong.

The model also indicated that the region could be considered as having pristine atmospheric conditions [9].

Ideally more days in August would have been included to further the investigation into biomass burning and dust aerosols, but unfortunately the investigation was restricted by instrument downtime. However, the CIMEL Electronique CE318 multiband sun photometer has been returned to South Africa and could potentially provide data from late August 2019, which can be used to measure overlapping time accurate data for further testing. The model generally provided a good fit between 400 nm to 890 nm, which is ideal for solar panel utilisation and power generation predictions.

The turbidity co-efficient for each day was calculated using the Ångstrom turbidity Equation 8.

$$\beta = \frac{\tau_{0.5}}{0.5^{-\alpha}} \qquad (8)$$

D: M: Y	τ (0.5 µm)	α_1	β
25 04 2018	0.025	0.90	0.013
05 05 2018	0.040	0.30	0.032
08 05 2018	0.055	0.60	0.036
26 05 2018	0.050	0.00	0.050
02 06 2018	0.005	0.00	0.005
06 06 2018	0.140	1.00	0.070
16 06 2018	0.020	0.00	0.020
27 06 2018	0.115	0.00	0.115
02 07 2018	0.100	1.20	0.044
18 07 2018	0.080	0.50	0.057
23 07 2018	0.045	0.50	0.032
28 07 2018	0.090	0.30	0.073
01 08 2018	0.055	0.30	0.045

Table 10: Aerosol optical depth, Ångstrom and turbidity values used to simulate the conditions for each day.

The Ångstrom turbidity co-efficient values represents the amount of aerosol present in a vertical direction within the atmosphere. Where $\beta < 0.1$ indicates a clear atmosphere and $\beta > 0.1$ would be indicative of a turbid atmosphere [10].

8.1.2 Spectral Comparison

There were visible spectral differences between the modelled and measured data sets such as;

- Strong O_2 absorption line at around 760 nm in the SMARTS modelled data.
- "Noise" or rapidly varying data in the SMARTS model, particularly in the 280 nm – 440 nm range, which could be attributed to the inherent difficulty of measuring spectra in the O_3 absorption bands.
- "Noise" in the measured data at the far ends of the upper and lower limits due to instrumentation design.
- The measured data appeared to have some calibration errors despite the instrumentation having been calibrated prior to use and still being well within the current calibration period. Such an error can be seen when looking at the two 'horns' at 660 nm and 680 nm.

It should be noted that the eater vapour absorption could have been reduced by removing the calculational dependence on temperature and relative humidity and manually entering values for water vapour, but it was decided against as it would not have been an overlapping time accurate input.

8.1.3 Aerosol Optical depth & Ångstrom parameter

As mentioned in 6.4 the model worked well with lower aerosol optical depth and Ångstrom values. A better RMSE could be achieved but resulted in overestimations of the broadband irradiance values. Exceptions occurred during July where the values were closer to that measured by AERONET.

An attempt was made at linking the low aerosol optical depth values at 500 nm to the conditions brought on by frontal activity, but no direct relationship could be positively established.

The relationship between Tables 5 and 9 occasionally converged between mid-June through July. Days with exceptionally low Ångstrom exponents indicated that there was no distinguishable change in aerosol optical depths below and above 500nm

Zero Ångstrom parameter values, such as those in Table 10 are indicative of large aerosol particles such as water or ice particles. A zero Ångstrom exponent values with a corresponding nonzero β value as in Equation 9.

$$IF\ \alpha = 0\ ;\ \beta \neq 0 \qquad (9)$$

The relationship between the Aerosol optical depth values across a specified range would have to be the same as can be seen in Equations 10 and 11.

$$\frac{\tau_1}{\tau_2} = \left(\frac{\lambda_1}{\lambda_2}\right)^{-0} = 1 \qquad (10)$$

$$\therefore\ \tau_1 = \tau_2 \qquad (11)$$

Given the season, it could also be large dust particles. Low Ångstrom parameter values were initially considered while earlier tests were conducted using the built-in aerosol models where the so-called "desert max" and "desert min" set of parameters provided the best fit with Ångstrom values from 0.18 to 0.6 [11]

9 Conclusion

From this investigation SMARTS appears to be a suitable model for simulating clear-sky direct beam and broadband irradiance. The programs performance will continue to be tested if overlapping time accurate data becomes available.

Acknowledgements

The data required to conduct the investigation belongs to and was provided by CSIR. The historical aerosol data which had been obtained from the AERONET database. The model used to conduct the investigation "SMARTS" was developed by C. Gueymard and his team.

References

[1] C. A. Gueymard, "The sun's total and spectral irradiance for solar energy applications and solar radiation models," *Sol. Energy*, vol. 76, no. 4, pp. 423–453, 2004.

[2] J. M. Pap and C. Fröhlich, "Total solar irradiance variations," *J. Atmos. Solar-Terrestrial Phys.*, vol. 61, no. 1–2, pp. 15–24, 1999.

[3] M. J. Brooks *et al.*, "SAURAN: A new resource for solar radiometric data in Southern Africa," *J. Energy South. Africa*, vol. 26, no. 1, pp. 2–10, 2015.

[4] E. Zawilska and M. J. Brooks, "An assessment of the solar resource for Durban, South Africa," *Renew. Energy*, vol. 36, no. 12, pp. 3433–3438, 2011.

[5] T. P. Fluri, "The potential of concentrating solar power in South Africa," *Energy Policy*, vol. 37, no. 12, pp. 5075–5080, 2009.

[6] C. Gueymard, "SMARTS2, A Simple Model of the Atmospheric Radiative Transfer of Sunshine: Algorithms and performance assessment," 1995.

[7] https://aeronet.gsfc.nasa.gov/cgi-bin/data_display_aod_v3?site=Pretoria_CSIR-DPSS&nachal=2&level=3&place_code=10

[8] https://aeronet.gsfc.nasa.gov/cgi-bin/webtool_aod_v3?stage=3&region=Southern_Africa&state=South_Africa&site=Pretoria_CSIR-DPSS&place_code=10&if_polarized=0

[9] Gueymard, C.A., 2005. SMARTS Code, Version 2.9. 5 User's Manual. *Solar Consulting Services. Available from http://www. solarconsultingservices. com/SMARTS295_manual. pdf.*

[10] Khoshsima, M., Bidokhti, A.A. and Ahmadi-Givi, F., 2014. Variations of aerosol optical depth and Angstrom parameters at a suburban location in Iran during 2009–2010. *Journal of earth system science*, *123*(1), pp.187-199.

[11] C. Gueymard, "The SMARTS spectral irradiance model after 25 years: New developments and validation of reference spectra", *Sol. Energy*, vol. 187, pp.233-235, 2019